Available online at www.sciencedirect.com
ScienceDirect
Cement and Concrete Research 36 (2006) 1508–1515
Cement and Concrete Research

Identification and quantification of cracks in concrete by optical fluorescent microscopy

Agnieszka Litorowicz

Institute of Fundamental Technological Research, Polish Academy of Sciences, Świętokrzyska 21, 00-049 Warszawa, Poland

Received 30 August 2005; accepted 19 May 2006

Abstract

Cracks in concrete structures can indicate major structural problems and can damage the appearance of monolithic construction. Cracking of concrete is a major factor affecting for the material strength and durability. The development of a crack pattern can contribute to increasing the permeability and the diffusivity of concrete, which is generally connected with a substantial reduction of its durability. This paper describes a method for identification and quantification of crack patterns in concrete by means of optical fluorescent microscopy and image analysis. Results obtained for undamaged and deteriorated specimens are presented. The range of investigation included several concrete mixes made in the laboratory. In order to induce cracks, concrete mixes were exposed to freezing action 0, 1 and 2 h after mixing. The concrete cubes of 100-mm and 150-mm size were frozen for 0 (reference specimens) and 2 days. Investigation of compressive strength, water permeability, chloride migration and analysis of cracks was made after 28 days. The low-temperature deteriorated specimens showed a significant reduction of compressive strength and resistance to water and chloride penetration in concrete. Correlations between density of cracks and compressive strength, depth of water penetration and depth of chloride penetration have been proposed.

Keywords: Crack detection; Image analysis; Compressive strength; Permeability

1. Introduction

The degradation of hydrated cement systems caused by various factors, often results in different levels and configurations of cracks in concrete, which influence the post-damage behaviour and qualities of concrete.

Fresh concrete may be susceptible to cracking during warm or cold conditions [1–5], especially if it is insufficiently cured. The tendency of concrete to cracking due to temperature changes during the hydration and hardening period has been known since the beginning of concrete technology.

Whatever the origin, if cracks occur, they play a major role in the mechanical behaviour, the permeability characteristics and the long term durability [4,6–10]. Quantitative investigation of the crack system in concrete can thus provide substantial insight into the deterioration of the concrete-based infrastructure. The most widely used techniques for studying cracks in concrete are scanning electron microscopy and optical microscopy [11–15]. Two tools are necessary to characterise cracks: one for observation and one for quantitative analysis. Recent developments in microscopy and image processing and analysis techniques provide powerful tools for quantitative microstructural investigation of concrete and allowed the crack pattern in these materials to be quantified.

In this investigation, a method for detection and quantification of cracks based on digital image analysis is introduced. The use of a resin impregnation technique in combination with the optical fluorescence microscopy and a computer image analysis technique provided a quantitative determination of the crack system.

2. Experimental program

2.1. Materials and specimens

Three commercially available Polish cements from Górażdże cement plant were used: CEM I 32.5R (Portland cement), CEM II/B-V 32.5R-HSR (with fly ash Class F according to ASTM C618-03 specification) and CEM III/A 32.5 NA (with slag).

E-mail address: akwiat@ippt.gov.pl.

0008-8846/$ - see front matter © 2006 Elsevier Ltd. All rights reserved.
doi:10.1016/j.cemconres.2006.05.011

Table 1
Composition of the concrete mixes

Materials	Mix designation		
	CEM I	CEM II	CEM III
	Content (kg/m^3)		
Cement CEM I 32.5R	331	–	–
Cement CEM II/B-V 32.5R	–	332	–
Cement CEM III/A 32.5 NA	–	–	331
Sand 0–2 mm	723	725	723
Crushed basalt 2–8 mm	623	624	622
Crushed basalt 8–16 mm	662	664	663
Water	179	180	179

Crushed basalt was used as coarse aggregate with fractions: 2–8 mm and 8–16 mm. Ordinary river sand with a maximum grain size of 2 mm was used as fine aggregate. The composition of concrete mixes is given in Table 1.

The concrete mixes were designed with constant water to cement ratio of 0.54. The concrete mixes were produced in a laboratory mixer (capacity 25 l). The workability and density were measured directly after mixing. All tests were performed according to Polish Standard PN-88/B-06250. The concrete was cast in 100×100×100-mm cube moulds for compression tests and in 150×150×150-mm cube moulds for water penetration tests, chloride migration tests and analysis of crack pattern.

In order to induce cracks, concrete mixes were exposed to freezing action immediately after mixing and at 1 and 2 h after mixing: the cubes were kept in the climatic chamber at a constant temperature of −5 °C. After 2 days of freezing, the specimens were demoulded and stored until the age of 28 days in high humidity conditions (RH>90%) and at temperature of 20 °C. The reference specimens (not subjected to freezing action) were demoulded 24 h after mixing and then stored in the same conditions.

2.2. Test methods

The range of the investigation covered the following tests.

2.2.1. Axial compression test

The compressive strength of four series of each concrete (reference, frozen immediately and 1 and 2 h after mixing) was determined on 100×100×100-mm cubes according to the Polish Standard PN-88/B-06250 (3 for each series).

2.2.2. Water penetration test

Water penetration test was performed according to the Polish Standard PN-88/B-06250 on 150-mm cubes. The initial water pressure of 0.2 MPa was applied and maintained for 24 h. Then, the pressure was increased by 0.2 MPa every 24 h up to 0.8 MPa. After splitting, the specimen perpendicular to the water exposed surface the maximum depth of water penetration was measured. As a result, the mean value of three specimens for each series was considered.

2.2.3. Chloride migration test

The chloride migration coefficient from non-steady-state migration experiment, determined according to Nordtest Method NT BUILD 492, is a measure of the resistance of the material to chloride penetration. A cylindrical specimen was drilled out from the half of 150-mm cube after testing water penetration and next a 50±2-mm-thick disc was sawn as the test specimen (Fig. 1).

The concrete disc (1 for each series) was placed between two solutions: one end of the disc in contact with an anolyte (0.3 N NaOH solution) and the other is in contact with a catholyte (10% NaCl solution). A potential was established between an anode immersed in the anolyte and a cathode immersed in the catholyte. The initial voltage was 30 V and after adjustment according to NT BUILD 492 the voltage was 50 V or 60 V. It was applied for approximately 24 h. After exposure, the concrete disc was split longitudinally and the depth to which chloride has penetrated into the sample was determined by the application of silver nitrate solution on the freshly split section, which coloured the areas containing chloride ions white. The non-steady-state migration coefficient was then calculated from Eq. (1):

$$D_{\mathrm{nssm}} = \frac{RT}{zFE}\frac{x-\alpha\sqrt{x}}{t} \tag{1}$$

where:

$$E = \frac{U-2}{L} \tag{2}$$

$$\alpha = 2\sqrt{\frac{RT}{zFE}}\cdot \mathrm{erf}^{-1}\left(1-\frac{2c_{\mathrm{d}}}{c_0}\right) \tag{3}$$

D_{nssm}	Non-steady-state migration coefficient (m^2/s)
z	Absolute value of ion valence (for chloride $z=1$)
F	Faraday constant, $F=9.648\times10^4$ [J/(V·mol)]
U	Absolute value of the applied voltage (V)
R	Gas constant, $R=8.314$ [J/(K·mol)]
T	Average value of the initial and final temperatures in the anolyte solution (K)
L	Thickness of the specimen (m)
x	Average value of the penetration depths (m)
t	Test duration (s)
erf^{-1}	Inverse of error function
c_{d}	Chloride concentration at which the colour changes ($c_{\mathrm{d}}\approx0.07$ N for OPC concrete)
c_0	Chloride concentration in the catholyte solution ($c_0\approx2$ N)

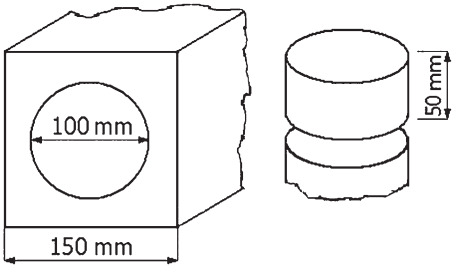

Fig. 1. Specimen drilling in a half of 150×150×150-mm cube after water penetration test.

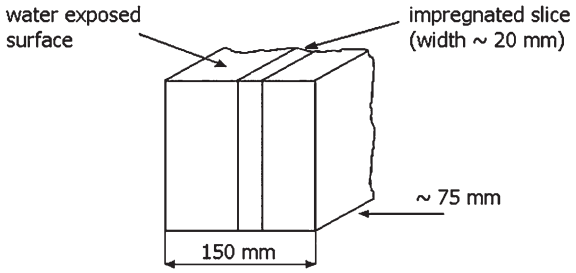

Fig. 2. Specimen cutting out of half of 150×150×150-mm cube after water penetration test.

2.3. Identification and quantification of crack system

2.3.1. Specimen preparation

The impregnated reground plane section (IRPS) technique [16], which is used at the IFTR laboratory for estimation of crack system in concrete, was transferred from DBT (Dansk Beton Technik) laboratory in Hellerup. For crack detection, concrete specimens were vacuum-impregnated according to the procedure described below:

1. Concrete cross-sections of 20 to 25 mm thickness were obtained using a diamond saw from half of 150-mm cubes after testing of water penetration. Specimens were prepared in such way that the surface to be examined was situated as closely as possible to the centre of half of cube perpendicular to the water exposed surface (Fig. 2).
2. The surfaces of the specimens were ground, polished and cleaned in order to remove surface irregularities produced by sawing and to obtain a smooth flat surface.
3. The specimens were dried in an oven at a temperature of 35 °C for 24 h.
4. The specimens were placed in a plastic bag and evacuated for at least 45 min at a constant pressure of −1 bar in a vacuum chamber.
5. The bag with samples inside was then filled with the epoxy resin containing fluorescent dye, which was introduced into the chamber while maintaining the vacuum.
6. The specimens submerged by the epoxy resin, were kept under vacuum for an additional 15 min.
7. Finally, the specimens were removed from the vacuum chamber and from the plastic bag, and cured in oven at the temperature of 35 °C for 24 h.The epoxy penetrated into the specimen and hardened in cracks and other defects. The excess of resin at the surface of specimen was removed by grinding down to 2 mm from the surface.

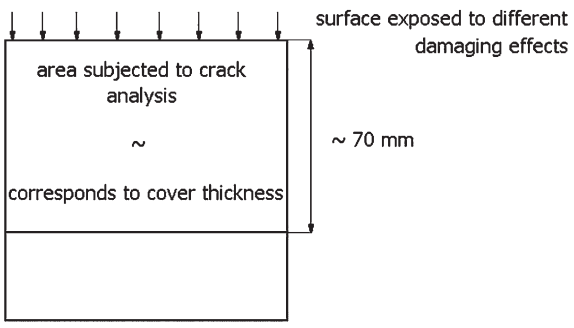

Fig. 3. Area of crack analysis.

Table 2
Characteristic of analyzed images

Magnification	Number of images in analyzed area	Size of image for sample		Size of a pixel
		100×100×20 mm	100×75×20 mm	
10×	2	25×61 mm	32×52 mm	8.4 μm

2.3.2. Levels of observation

Two levels of crack observation in concrete in ultraviolet light were applied. At the macroscopic level without a microscope, large cracks were identified. This allowed a quick indication of major defects in the concrete. Microscopic observation of the impregnated reground polished specimens (IRPS) by means of an optical microscope at a magnification of 10× was sufficient to detect fine cracks. When applied to ordinary concrete, the technique generates images with a good contrast, which are convenient for quantitative analysis.

2.3.3. Digital crack identification and analysis

The IRPS were subjected to observation in ultraviolet light using a Nikon optical microscope at a magnification of 10 times. All the images reported in this study were acquired by a Sony DXC-950P video camera attached to the microscope. Identification of cracks in impregnated specimens was carried out on the digital images by means of Image Pro Plus image analysis system. The images were acquired in area of specimen surface showed in Fig. 3. The number of images taken from one area and size of image for two kinds of specimen is given in Table 2.

Fig. 4 shows typical image of a concrete specimen. To assess the characteristics of the crack network, the colour image was converted into a binary image (Fig. 4b) on the basis of its R (red), G (green) and B (blue) components by means of a segmentation process. The threshold level for crack

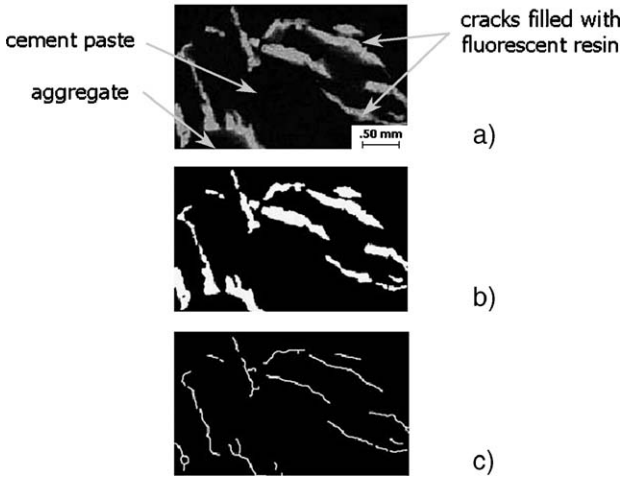

Fig. 4. The image processing stages: (a) original colour image, (b) binary image after thresholding and (c) binary image after skeletonization.

identification (brightest phase in the image—fluorescent resin) in this case was set between: R: 0–255, G: 120–255, B: 0–255. After filtering operations on the binary image and classification of objects according to shape criteria as described in [4], cracks were distinguished from other features. The final step of image processing was to reduce the cracks to single pixel lines by binary thinning—filter known as skeletonization (Fig. 4c).

To distinguish and describe the crack patterns in the concrete specimens, six parameters were used:

1. Angle—the angle between the vertical axis and the major axis of the ellipse equivalent to the object, where $0° \le \text{angle}° \le 180°$.
2. Area—the area of each object (any holes in object are not included to object area).
3. Dendritic length—the total length of all the one-pixel-thick branches.
4. Per Area—the ratio between the area of the counted object and the entire area of the active image.
5. Radius Ratio—the ratio between max radius and min radius for each object.
6. Roundness—determined for each objects by the following formula: perimeter^2/4*Π*area. Roundness of circular objects = 1; others shapes > 1.

The degree of crack orientation was determined on the basis of the classical stereological method of oriented secants on a plane [17,18]. The automatic procedure elaborated for the estimation of crack pattern orientation included logical binary operations between two images: the image of the crack network in concrete and an image of parallel equidistant lines with a given direction (Fig. 5). A set of parallel equidistant lines with a given direction was superimposed on an image and the number N of intersections of the cracks with the set of lines was measured. The number of intersections $N_L(\Theta)$ for a total length of lines L was obtained. By rotating the set of reference lines from 0° to 180° by 15° steps, a series of $N_L(\Theta)$ values was obtained. These values can be represented by means of rose of intercepts. The degree of orientation was computed according to Eq. (4):

$$\omega = \frac{(N_{L\max} - N_{L\min})}{N_{L\max} + \left(\frac{\Pi}{2} - 1\right) \cdot N_{L\min}}, \quad 0 \le \omega \le 1 \tag{4}$$

where: ω—degree of orientation, $N_{L\max}$—maximum values taken by $N_L(\Theta)$ when (Θ) varies, $N_{L\min}$—minimum values taken by $N_L(\Theta)$ when (Θ) varies. Degree of orientation ω takes the value 0 for a perfectly isotropic crack pattern and the value 1 when all the cracks have the same orientation.

In order to estimate the crack width distribution an automatic procedure was prepared. First, cracks on the binary image were subjected to a sorting operation. During the sorting process, the objects were rotated automatically so that their major axis were aligned vertically and the objects were positioned in rows. Then a logical operation was applied between the image with sorted cracks and an image of parallel equidistant lines perpendicular to the cracks. The consequence of the logical operation was an image of intersections of cracks with the lines (Fig. 6). Intersections represented line segments whose length corresponded to the crack width. The results were presented as the percentage of objects in the given range of crack widths.

In this way, for each concrete specimen, it is possible to determine:

1. Dendritic length of cracks—L (mm)—total length of all the skeletonized cracks in the image.
2. Area of cracks—A (mm^2)—total area of cracks on the image.
3. Average width of cracks—W (mm)—total cracks area divided by total dendritic length.
4. Crack density—L_A (mm/mm^2)—total dendritic length of cracks per image area.

Fig. 5. Estimation of crack pattern orientation by means of the oriented secants method—logical binary operations between two images.

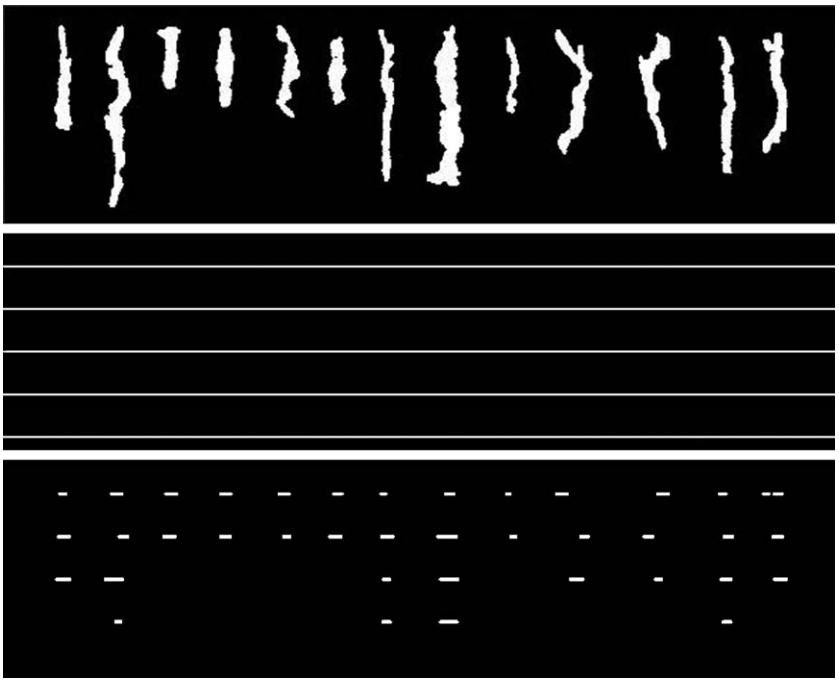

Fig. 6. Logical operation of crack image and image of parallel lines.

5. Areal fraction—A_A (mm^2/mm^2)—ratio between the area of the counted cracks to the entire area of the active image.
6. Degree of crack orientation—shown by means of "rose of intercepts".
7. Distribution of crack width—shown as percentage object fraction in the given range of crack width.

3. Results and discussion

3.1. Compressive strength

Table 3 presents the 28-day compressive strength data. The strength is given as an average value f_c of three measurements in each series. As expected, the concrete made with Portland cement CEM I had the highest strength after 28 days in comparison with concretes CEM II (cement with fly ash) and CEM III (cement with slag). The strengths of concretes exposed to − 5 °C showed decreasing reduction of compressive strength with retardation of initial freezing age of concrete mixes.

Table 3
Compressive strength of concrete after 28 days

Concrete mix	Compressive strength (MPa)			Mean value f_{c28} (MPa)
	Specimen 1	Specimen 2	Specimen 3	
CEM I	45.45	46.35	45.63	45.81
CEM Im0	26.19	25.65	25.38	25.74
CEM Im1	27.81	27.90	28.26	27.99
CEM Im2	29.16	29.79	30.78	29.91
CEM II	35.10	35.10	35.37	35.19
CEM IIm0	22.14	21.60	22.32	22.02
CEM IIm1	26.46	26.64	26.37	26.49
CEM IIm2	26.37	27.09	27.36	26.94
CEM III	42.57	40.95	41.58	41.70
CEM IIIm0	30.33	30.51	29.61	30.15
CEM IIIm1	36.18	35.37	35.82	35.79
CEM IIIm2	37.17	36.00	36.99	36.72

m0—concrete frozen after mixing, m1—concrete frozen 1 h after mixing, m2—concrete frozen 2 h after mixing.

3.2. Water penetration test

Depth of water penetration under pressure was determined on specimens after low-temperature deterioration and on reference specimens (Table 4). It can be observed that the water penetration depth for undamaged concrete CEM II was the smallest, 21 mm. For concretes CEM I and CEM III, the depth of water penetration was about two times larger. Low-temperature damage significantly decreased the resistance to water penetration under pressure: the largest penetration depth was obtained for CEM IIm0, while the smallest reduction was

Table 4
The depth of water penetration in concrete after freezing of fresh mix

Concrete mix	Depth of water penetration (mm)			Mean value (mm)
	Specimen 1	Specimen 2	Specimen 3	
CEM I	46	30	38	38
CEM Im0	142	143	134	140
CEM Im1	135	132	133	133
CEM Im2	120	127	122	123
CEM II	21	22	19	21
CEM IIm0	150	150	150	150
CEM IIm1	141	150	140	144
CEM IIm2	115	148	110	124
CEM III	39	45	34	39
CEM IIIm0	97	88	80	88
CEM IIIm1	47	48	60	52
CEM IIIm2	52	47	45	48

Table 5
Results of chloride migration coefficient

Concrete mix	Chloride penetration depth (mm)	Migration coefficient ($\times 10^{-12}$ m^2/s)
CEM I	23.71	6.05
CEM Im0	53.71	14.20
CEM Im1	39.00	12.23
CEM Im2	37.14	9.88
CEM II	13.00	3.21
CEM IIm0	21.14	5.47
CEM IIm1	18.29	5.57
CEM IIm2	16.14	4.83
CEM III	13.29	3.28
CEM IIIm0	19.43	5.97
CEM IIIm1	14.86	4.45
CEM IIIm2	13.71	4.05

Table 6
Results of crack pattern analysis (150×150×150 mm cubes after water penetration test)

Concrete mix	Total length (mm)	Area (mm^2)	Average width (mm)	Density (mm/mm^2)	Degree of orientation
CEM Im0	494.7	38.8	0.078	0.30	0.17
CEM Im1	449.0	35.5	0.079	0.27	0.19
CEM Im2	386.6	30.7	0.080	0.23	0.16
CEM IIm0	681.1	55.5	0.081	0.41	0.24
CEM IIm1	542.6	40.6	0.075	0.33	0.25
CEM IIm2	411.4	33.0	0.082	0.25	0.20
CEM IIIm0	283.3	22.5	0.079	0.17	0.18
CEM IIIm1	258.0	20.0	0.077	0.16	0.16
CEM IIIm2	233.0	18.6	0.079	0.14	0.17

for CEM IIIm2. Concrete CEM IIm0 was not resistant to water permeability–water leakage through the specimens was observed. In low-temperature deteriorated concretes, the resistance to water penetration increased with retardation of initial freezing age of concrete mixes.

3.3. Chloride migration test

It can be seen in Table 5 that the reference concrete CEM I (Portland cement) shows higher chloride penetration than the reference concretes CEM II (cement with fly ash) and CEM III (cement with slag), which agrees with other results in the literature [19,20]. Concrete containing mineral additions exhibited higher resistance to chloride ion penetration than concrete with plain Portland cement. Chloride penetration depths and chloride migration coefficients of the reference concretes are lower in comparison with concretes subjected to freezing action. Differences in the migration coefficient values between reference and damaged concretes are larger for CEM I than for CEM II and CEM III. Concretes subjected to freezing action showed decreased depth of chloride penetration with retardation of initial freezing age of concrete mixes.

3.4. Analysis of crack pattern

The cracks were observed only in the low-temperature deteriorated concrete. Table 6 gives the crack characteristics of the samples sawn from the 150-mm cubes subjected previously to the water penetration test. The deteriorated series of concrete CEM II showed the highest crack density, while the lowest crack density was found in series of concrete CEM III. In the analysed concretes, the average crack width was similar in the range from 0.075 mm to 0.082 mm. The degree of orientation revealed that the cracks are randomly oriented and there is not a definite orientation in the crack pattern. As it is seen from Table 6, the sooner the beginning of freezing was after mixing, the higher was the crack density.

The distribution of crack widths is presented in Figs. 7, 8 and 9 as an average value of measurements performed on three samples in each deteriorated series of concretes CEM I, CEM II and CEM III. For concrete CEM I and CEM II, the distribution of crack widths is similar. The most of the objects are in the range of crack widths from 0.025 mm to 0.100 mm. In concrete CEM III, the distribution of crack widths is moved slightly toward smaller widths. More objects are included in range of crack widths up to 0.025 mm and less in the range from 0.100 mm to 0.125 mm in comparison with concrete CEM I and CEM II.

As seen from Fig. 10, a relationship between the compressive strength and density of cracks was found. The compressive

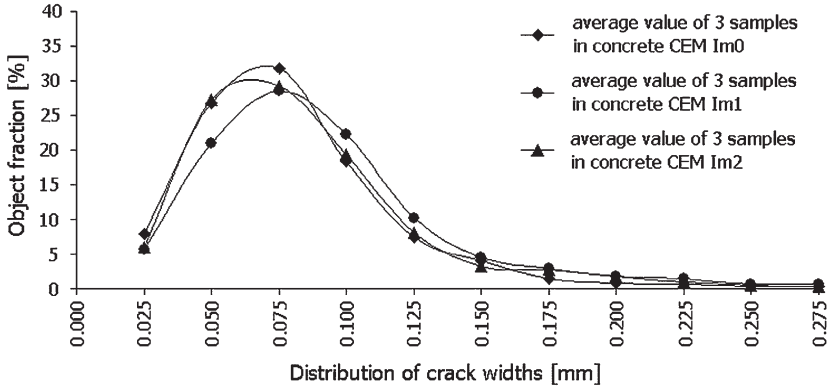

Fig. 7. Distribution of crack widths in samples of concrete CEM I exposed to frost action before hardening.

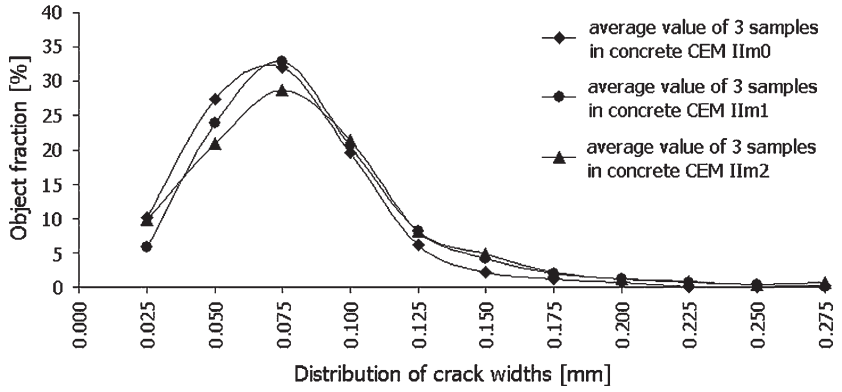

Fig. 8. Distribution of crack widths in samples of concrete CEM II exposed to frost action before hardening.

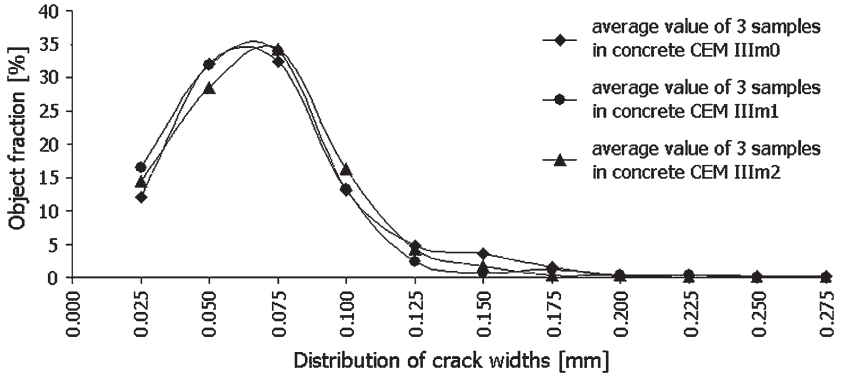

Fig. 9. Distribution of crack widths in samples of concrete CEM III exposed to frost action before hardening.

strength of concrete decreased with an increase of crack density for each analyzed concrete.

The predominant effect of crack density on the depth of water penetration is distinct for analyzed concretes, especially for CEM I and CEM II. In spite of using different types of cement, the test data fit into one curve (Fig. 11). There is a high correlation between the depth of water penetration and the density of cracks.

No correlation was observed between the depth of water penetration and the degree of orientation or width of cracks. From Refs. [7,21], it was noted that in the range of small cracks, up to about 0.1 mm, cracking had a little effect on concrete permeability.

Fig. 12 shows the correlation between the depth of chloride penetration and the density of cracks. As expected, the chloride penetration increased with an increase of crack density. But a

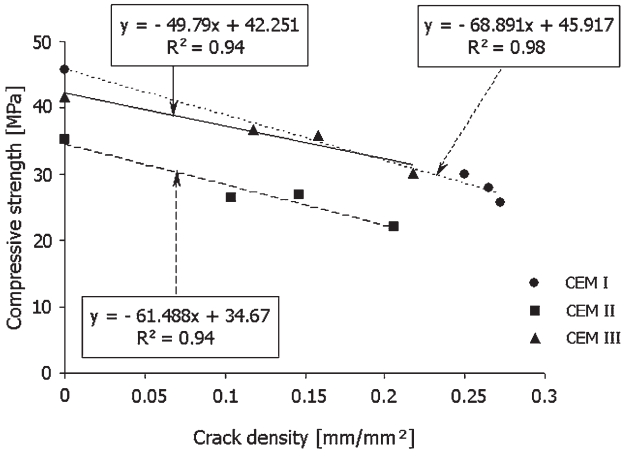

Fig. 10. The relationship between the crack density and the compressive strength of concrete samples exposed to frost action before hardening.

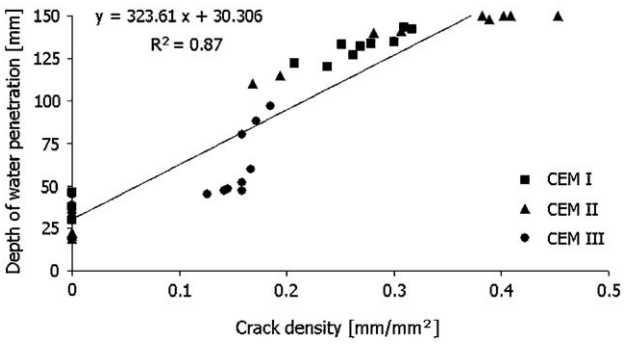

Fig. 11. The relationship between the crack density and the depth of water penetration in concrete.

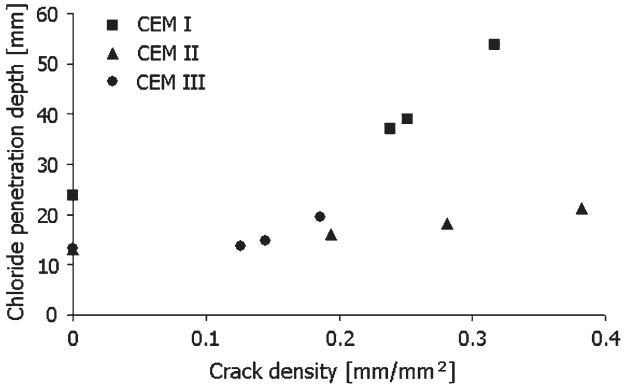

Fig. 12. The relationship between the crack density and the depth of chloride penetration in concrete.

relationship between the depth of chloride penetration and the degree of orientation or width of cracks was not noticed.

It appears that in examined heavily deteriorated (cracked) concretes the resistance to water and chloride ion penetration significantly depends on the density of cracks.

4. Conclusions

A method for the identification and quantification of crack patterns in concrete by means of optical fluorescent microscopy and image analysis system was elaborated using impregnated reground polished sections. Observation of the concrete surface in ultraviolet light using an optical microscope at a magnification of 10 times is sufficient to detect fine cracks. The applied technique generates images with a good contrast, which are convenient for automatic quantitative analysis.

The data obtained by means of image analysis methods are unavailable using conventional test procedures. The proposed method provides a quantitative determination of the crack system using parameters such as: dendritic length, area, average width, density, area fraction, degree of orientation and distribution of crack widths. Evidence for concrete damage due to freezing during the hydration and hardening period was obtained.

The compressive strength of concrete subjected to low-temperature action after mixing was significantly reduced in relation to the compressive strength of reference concrete. The depth of water and chloride penetration in concrete increased in damage specimens. In concretes exposed to − 5 °C, the reduction of the compressive strength and the resistance to water and chloride penetration depends on the retardation of initial freezing age of concrete mixes. The sooner concrete mixes were exposed to low temperature the larger the reduction of their properties. A correlation between the density of cracks and compressive strength, depth of water penetration and depth of chloride penetration was found.

This method can be used for quantification of cracks in concrete specimens made in the laboratory and also in elements sawn out from existing concrete structures damaged by various mechanisms.

Acknowledgement

This project was financially supported by KBN Grant No. 5 T07E 06125.

References

[1] C. Qi, J. Weiss, J. Olek, Characterization of plastic shrinkage cracking in fiber reinforced concrete using image analysis and a modified Weibull function, Materials and Structures 36 (2003) 386–395.
[2] K. Wang, S.P. Shah, P. Phuaksuk, Plastic shrinkage cracking in concrete materials—influence of fly ash and fibers, ACI Materials Journal 98 (2001) 458–464.
[3] Y. Ma, M. Tan, K. Wu, Effect of different geometric polypropylene fibers on plastic shrinkage cracking of cement mortars, Materials and Structures 35 (2002) 165–169.
[4] M.A. Glinicki, A. Litorowicz, Application of UV image analysis for evaluation of thermal cracking in concrete, in: A.M Brandt, V.C. Li, I.H. Marshall (Eds.), Proceedings of Seventh International Symposium on Brittle Matrix Composites BMC 7, Warsaw, 2003, pp. 101–109.
[5] S. Lykke, E. Skotting, U. Kjær, Prediction and control of early-age cracking: experiences from the Øresund Tunnel, Concrete International 22 (2000) 61–65.
[6] H.R. Samaha, K.C. Hover, Influence of microcracking on the mass transport properties of concrete, ACI Materials Journal 89 (1992) 416–424.
[7] C.-M. Aldea, S.P. Shah, A. Karr, Permeability of cracked concrete, Materials and Structures 32 (1999) 370–376.
[8] H. Mihashi, T. Nishiwaki, J.P. Leite, Effectiveness of crack control on durability of HPFRCC, in: A.E. Naaman, H.W. Reinhardt (Eds.), Proceedings of the Fourth International RILEM, Ann Arbor, 2003, pp. 437–450.
[9] N. Gowripalan, V. Sirivivatnanon, C.C. Lim, Chloride diffusivity of concrete cracked in flexure, Cement and Concrete Research 30 (2000) 725–730.
[10] P.P. Win, M. Watanabe, A. Machida, Penetration profile of chloride ion in cracked reinforced concrete, Cement and Concrete Research 34 (2004) 1073–1079.
[11] H.Chr. Gran, Fluorescent liquid replacement technique. A means of crack detection and water:binder ratio determination in high strength concretes, Cement and Concrete Research 25 (1995) 1063–1074.
[12] M. Elzafraney, P. Soroushian, Assessment of microcrack development in concrete materials of different strengths, Materials and Structures 274 (2004) 724–731.
[13] K.M. Nemati, P. Stroeven, Stereological analysis of micromechanical behavior of concrete, Materials and Structures 34 (2001) 486–494.
[14] P. Soroushian, M. Elzafraney, A. Nossoni, Specimen preparation and image processing and analysis techniques for automated quantification of concrete microcracks and voids, Cement and Concrete Research 33 (2003) 1949–1962.
[15] A. Ammouche, J. Riss, D. Breysse, J. Marchand, Image analysis for the automated study of microcracks in concrete, Cement and Concrete Composites 23 (2001) 267–278.
[16] A. Henrichsen, P. Laugesen, Monitoring of concrete quality in high performance civil engineering constructions, in: S. Diamond, et al., (Eds.), Microstructure of Cement Based Systems/Bonding and Interfaces in Cementitious Materials, MRS, vol. 370, 1994, pp. 49–56.
[17] S.A. Sałtykow, Stereometrische Metallographie, VEB Deutschen Verlag für Grundstofferindustrie, Leipzig, 1976.
[18] P. Stroeven, Some aspects of micromechanics of concrete, PhD Thesis, Stevin Laboratory, Technological University of Delft, 1973.
[19] C.C. Yang, S.W. Cho, R. Huang, The relationship between charge passed and the chloride-ion concentration in concrete using steady-state chloride migration test, Cement and Concrete Research 32 (2002) 217–222.